Controllable transport of a skyrmion in a ferromagnetic narrow channel with voltage-controlled magnetic anisotropy

Junlin Wang[1,2,3]**, Jing Xia**[1]**, Xichao Zhang**[1,2]**, G. P. Zhao**[4]**, Jing Wu**[5]**, Yongbing Xu**[2,3]**, Lei Ye**[6]**, Zhigang Zou**[7] **and Yan Zhou**[1]

[1] School of Science and Engineering, The Chinese University of Hong Kong, Shenzhen 518172, China

[2] School of Electronic Science and Engineering, Nanjing University, Nanjing 210093, China

[3] Department of Electronic Engineering, University of York, York, YO10 5DD, United Kingdom

[4] College of Physics and Electronic Engineering, Sichuan Normal University, Chengdu 610068, China

[5] Department of Physics, University of York, York, YO10 5DD, United Kingdom

[6] College of Communication Engineering, Chongqing University, Chongqing, 400044 China

[7] Eco-materials and Renewable Energy Research Center(ERERC), National Laboratory of Solid State Microstructures, Department of Physics, Nanjing University, Nanjing 210093, China

E-mail: yongbing.xu@york.ac.uk, zhouyan@cuhk.edu.cn

December 2017

Abstract. Magnetic skyrmions have potential applications in next-generation spintronics devices with ultralow energy consumption. In this work, the current-driven skyrmion motion in a narrow ferromagnetic nanotrack with voltage-controlled magnetic anisotropy (VCMA) is studied numerically. By utilizing the VCMA effect, the transport of skyrmion can be unidirectional in the nanotrack, leading to a one-way information channel. The trajectory of the skyrmion can also be modulated by periodically located VCMA gates, which protects the skyrmion from destruction by touching the track edge. In addition, the location of the skyrmion can be controlled by adjusting the driving pulse length in the presence of the VCMA effect. Our results provide guidelines for practical realization of the skyrmion-based information channel, diode, and racetrack memory.

1. Introduction

Magnetic skyrmions are nanoscale particle-like topological configurations, which have been found in certain magnetic bulks, films and nanowire [1–8]. The skyrmion is stabilized by delicate competitions among the ferromagnetic exchange coupling, perpendicular magnetic anisotropy (PMA) and Dzyaloshinskii-Moriya interaction (DMI) in magnetic systems [9–14]. Magnetic skyrmions are expected to be used as information carriers in the next-generation spintronic devices due to their low-power consumption and small sizes [15–26]. The skyrmion can be driven by the spin polarized current and spin hall torque are investigated widely[27]. The external effects on the velocity and trajectory of the skyrmion in nanodevice are also reported [31].

The skyrmion Hall effect(SkHE) is one of the most significant obstacle to the high-speed transmission of skyrmions in confined geometries. The SkHE is previously theoretiacally predicted and has been observed experimentally[28, 29]. The SkHE is caused by the Magnus force acting on the transporting skyrmion with a topological number of Q = ± 1. The SkHE display a detrimental effect which makes the skyrmion deviate from the desired transmission path. One promising approach is to modulate the magnetic anisotropy in skyrmion racetrack memory and avoid skyrmion break at the edge of nanotrack[30–32].

In this paper, we report the dynamics of a skyrmion in a narrow ferromagnetic nanotrack channel with voltage-controlled perpendicular magnetic anisotropy(VCMA), which can be used to build the skyrmion diode and ratchet memory [33, 34] and avoid from the SkHE. The pinning and depinning of the magnetic skyrmion in the nanotrack through the VCMA gate are investigated. This work will be useful for the design and development of the skyrmion transport channel, which is a building block for any future skyrmion-based information devices.

2. Model and simulations

The simulation model is an ultrathin ferromagnetic nanotrack, 1000 nm $\times$ 80 nm $\times$ 0.4 nm, as shown in Fig. 1a. The model is discretized into tetragonal volume elements with the size of 2 nm $\times$ 2 nm $\times$ 0.4 nm. The micromagnetic simulations are performed with the Object Oriented MicroMagnetic Framework (OOMMF) [35]. The dynamic of magnetization are described by Landau-Lifshitz-Gilbert LLG (LLG) equation, written as

$$\frac{dm}{dt} = -\gamma_0 m \times h_{\text{eff}} + \alpha(m \times \frac{dm}{dt}) - um \times (m \times p), \tag{1}$$

where m is the reduced magnetization $\frac{M}{M_S}$, M_S is the saturation magnetization. γ_0 is the gyromagnetic ratio and α is the damping coefficient. h_{eff} is the effective field including the contributions of Heisenberg exchange, Dzyaloshinskii-Moriya interaction (DMI), magnetic anisotropy and demagnetization field. The u can be defined as $\frac{\gamma_0 \hbar j P}{2de\mu_0 M_S}$, $\hbar$ is the reduced Plank constant, j is the current density, $P = 0.08$ is the spin Hall angle, a is the atomic lattice constant, e is the electron charge, μ_0 is the vacuum permeability constant, d is the thickness of the magnetic nanotrack[36]. p is the direction of the spin polarization which is
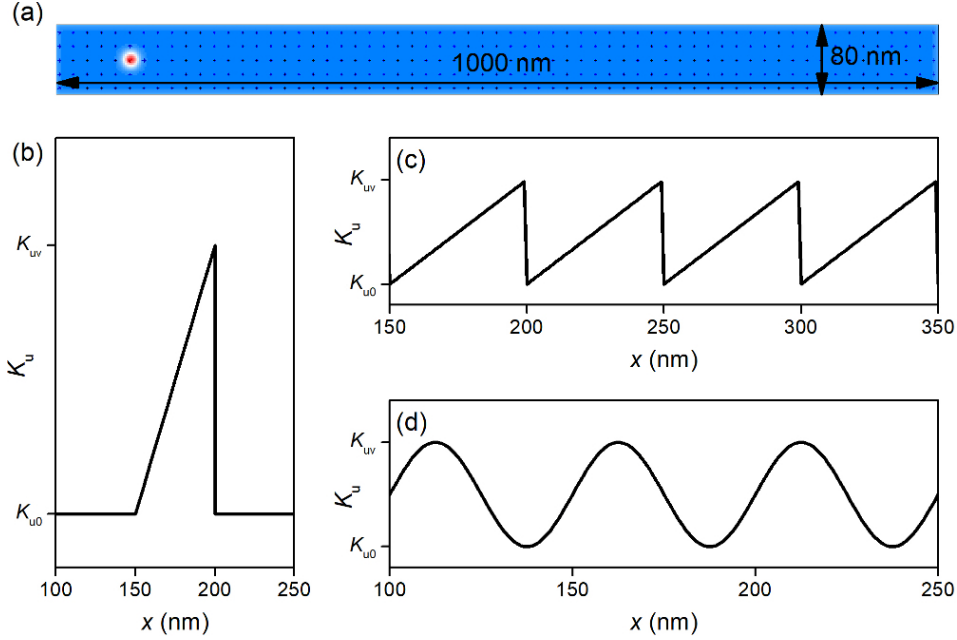
Figure 1. (a) A Schematic of the magnetic nanotrack where a magnetic skyrmion is initially placed. The out-of-plane magnetization component is represented by the red $(-z)$-white (0)-blue $(+z)$ color scale. (b) A linear anisotropy profile. (c) A periodical repetition of a linear anisotropy profile with a period w. (b) Sinusoidal function of x with a period w.

equal to $-\hat{y}$. The parameters for the micromagnetic simulation are adopted from Ref. [37]: the saturation magnetization $M_S = 580$ kA/m, the damping coefficient $\alpha = 0.3$, the DMI constant $D = 3$ mJ/m^2, and the exchange constant $A = 15$ pJ/m. In the simulation, the profile of the voltage-controlled magnetic anisotropy (VCMA) in the nanotrack are shown in Figs. 1b-d. For the simulation of the pinning/depinning states of the skyrmion, the PMA profile is shown in Fig. 1b. VCMA linearly varies from K_{u0} to K_{uv} and $K_{u0} = 0.8$ MJ/m^3. For the simulation of the motion of skyrmion, two types of VCMA profile are considered, period wedge-shape and sinusoidal functions, as shown in Figs. 1c and d respectively. The function for the period wedge-shape profile is given as:

$$K_u(x) = K_{u0} + K_{uv} - K_{u0}wx, \tag{2}$$

$$K_u(x) = K_{u0} + K_{uv} - K_{u0}2(1 + \sin(2\pi x/w - \varphi)), \tag{3}$$

where w is the period length w, φ is the phase, and x is the longitudinal coordinate. The period wedge-shape is given in the Eq. 2 and the sinusoidal function is given in the Eq. 3. The linear anisotropy profile and the sinusoidal function profile are given in the Figs. 1b and c.

3. Results and discussion

3.1. The pinning/depinning states of isolate skyrmion in nanotrack

Fig. 2 shows the pinning/depinning states of isolate skyrmion driven by the spin current in a nanotrack with the PMA profile shown in Fig. 1b. Fig. 2a and b show the effect of the
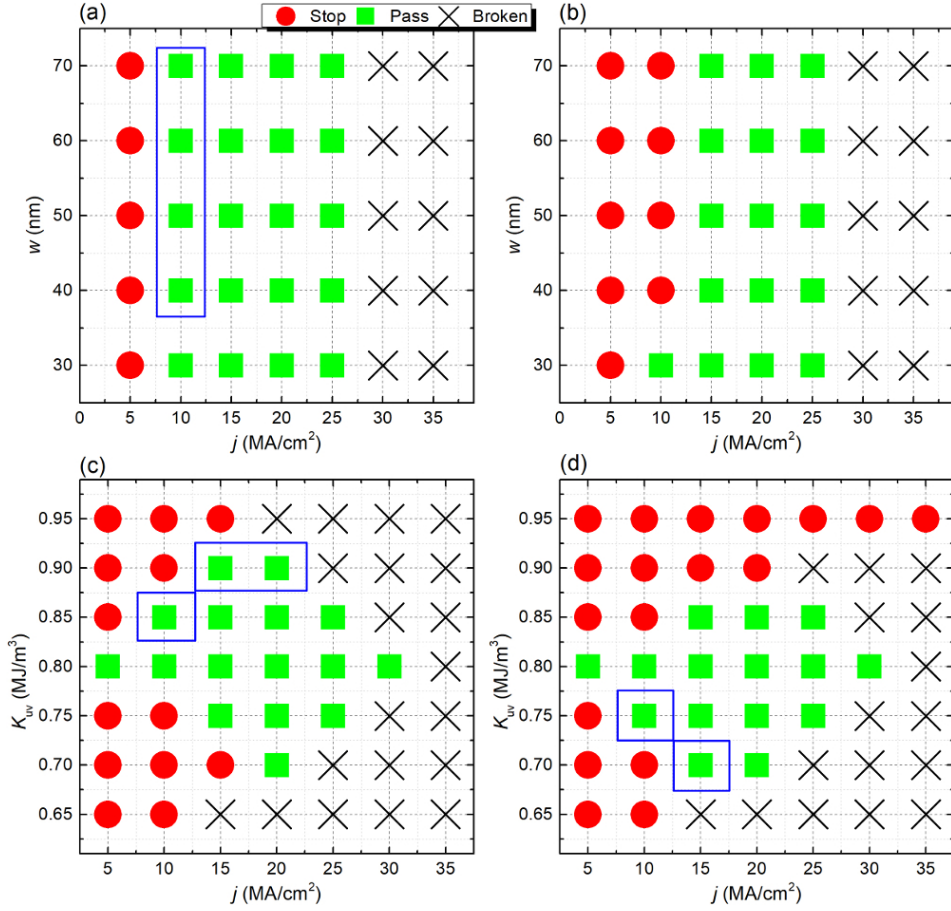
Figure 2. The pinning/depinning states of an isolate skyrmion driven by the current in a magnetic track. (a), (b) The pinning/depinning states of a skyrmion at various width w and driving current j along $+x$ and $-x$ axis for $K_{uv} = 0.85$ MJ/m^3, respectively. (c), (d) The pinning/depinning states of a skyrmion at various K_{uv} and j along $+x$ and $-x$ axis for the fixed $w = 50$ nm, respectively. The solid circle means the skyrmion is not able to pass the well or barrier, the solid square means the skyrmion can pass the well or barrier and the cross means the skyrmion is destroyed.

width and the current density on the pinning/depinning states. Initially, the relaxed skyrmion is located at the left side of the VCMA region when the spin current is applied along $+x$ axis. The skyrmion is not able to pass the VCMA region when the current density is smaller than 10 MA/cm^2 and pass the VCMA region when 25 MA/cm$^2 < j < 30$ MA/cm^2. The skyrmion will be destroyed when the current is larger than 30 MA/cm^2. When the spin current is applied along $-x$ axis, the skyrmion is located at the right side of the VCMA region. Most states are the same to the corresponding results in Fig. 1a, except for the case of $j = 10$ MA/cm^2. For $j = 10$ MA/cm^2 and w > 30 nm, the skyrmion can pass the VCMA region when the current is applied along $+x$ axis while it can not pass when the current is applied along $-x$ axis. It means that the skyrmion can pass only in one direction, $+x$ axis. The motion of skyrmion is unidirectional. The parameters corresponding to the unidirectional pass along $+x$ axis are marked with blue box in Fig. 2a. Fig. 2c and d show the effect of the VCMA and the current density on the pinning/depinning states. The results shows that the states is sensitive to the
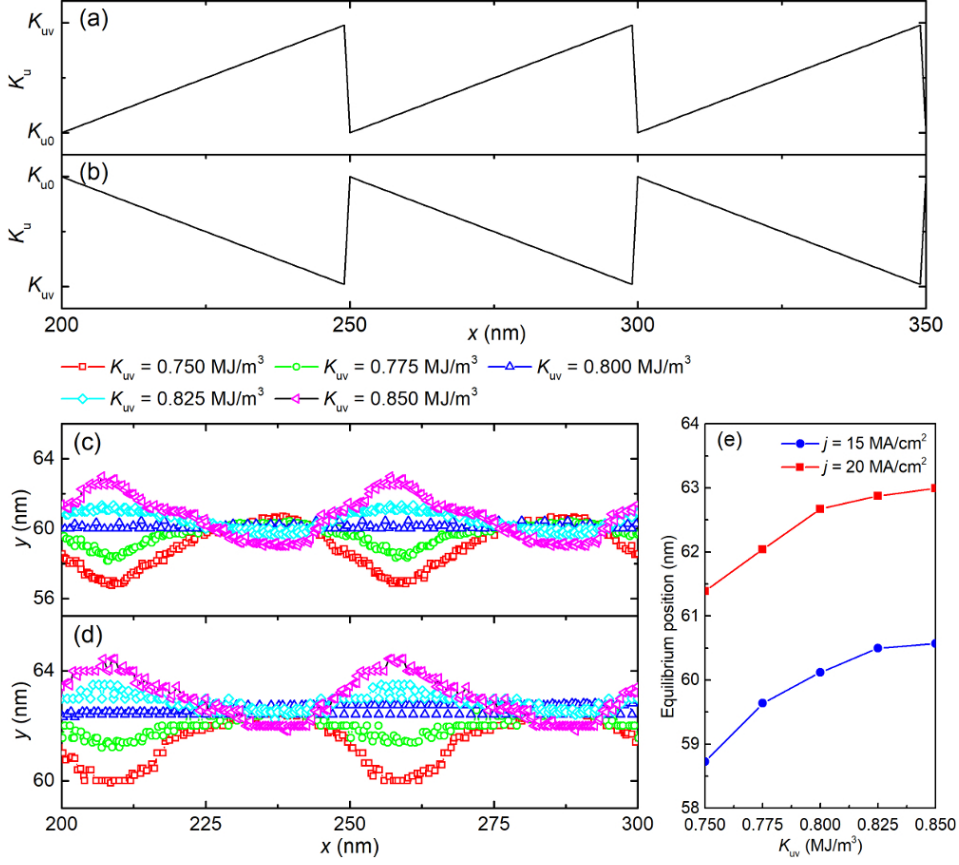
Figure 3. (a) The wedge-shaped profile of K_u for $K_{uv} > K_{u0}$. (b) The wedge-shaped profile of K_u for $K_{uv} < K_{u0}$. (c) The trajectories of the skyrmion in the nanotrack with various K_{uv} for $j = 15$ MA/cm^2. (d) The trajectories of the skyrmion in the nanotrack with various K_{uv} for $j = 20$ MA/cm^2. (e) The equilibrium position of the skyrmion in the y direction for (b) and (c). The spin current is applied along $+x$ axis.

VCMA. The unidirectional behaviors also can be found. The parameters for the unidirectional pass along $+x$ axis are marked with blue box in Fig. 2c and these for the unidirectional pass along $-x$ axis are marked with blue box in Fig. 2d. The unidirectional behaviors show that the voltage gate can be used to build skyrmion diode.

3.2. Skyrmion motion with the spatially dependence of VCMA gate

The skyrmion motion driven by the spin current in a magnetic nanotrack with the spatially dependence of VCMA is simulated. The VCMA is periodical repetition of a wedge-shape profile, as shown in Fig. 3a ($K_{uv} > K_{u0}$) and b ($K_{uv} > K_{u0}$). Initially, the relaxed skyrmion is located at $x = 86$ nm and $y = 40$ nm. The trajectories of the skyrmion driven by the spin current ($j = 15$ MA/cm^2) in the nanotrack with various K_{uv} are shown in Fig. 3c. For $K_{uv} = 0.800$ MJ/m^3, a uniform perpendicular magnetic anisotropy in the nanotrack, the skyrmion shows a transverse motion towards to the upper edge resulted by the transverse force due to skyrmion Hall effect firstly [29]. When the transverse force and edge-skyrmion repulsive force are balanced, the skyrmion moves straightly [13, 14, 20]. It can be seen that the
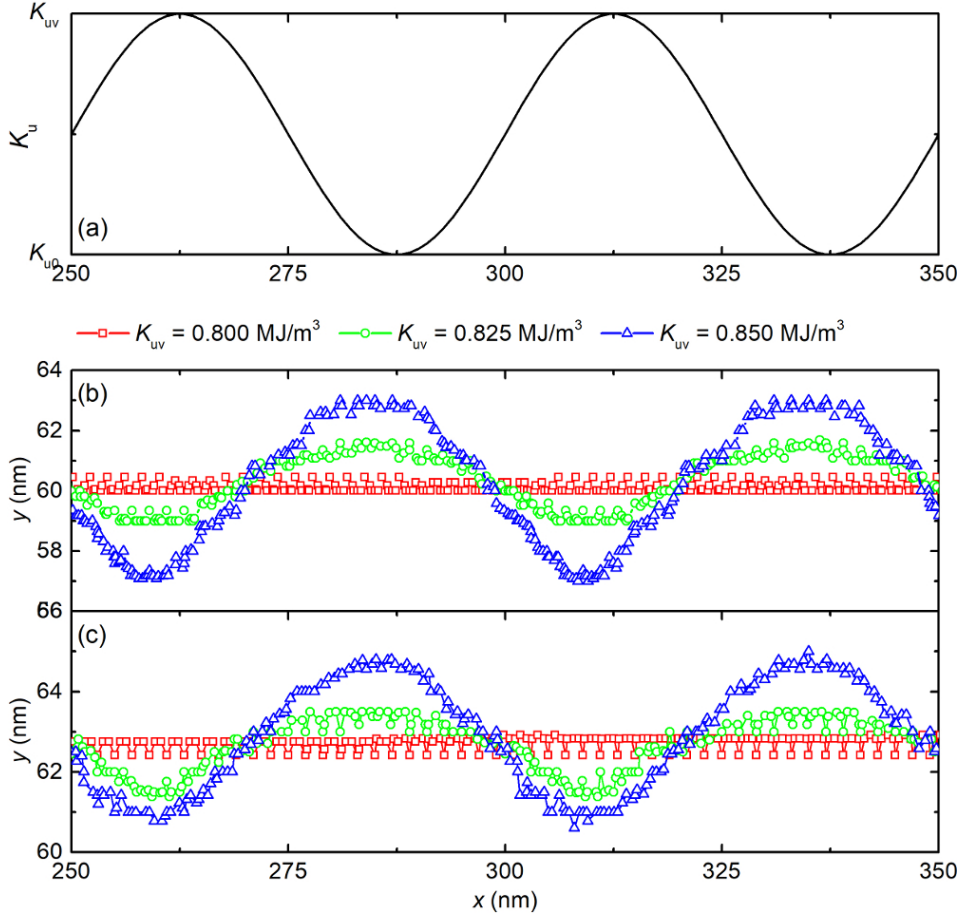
Figure 4. (a) The profile of K_u as a sinusoidal function of x. (b) The trajectories of the skyrmion in the nanotrack with various K_{uv} for $j = 15$ MA/cm^2. (c) The trajectories of the skyrmion in the nanotrack with various K_u for $j = 20$ MA/cm^2. The spin current is applied along $+x$ axis.

skyrmion moves straightly at $y = 60$ nm finally. For $K_{uv} = 0.850$ MJ/m^3, the skyrmion moves in a periodical wavy trajectory with an equilibrium position at $y = 60.6$ nm. Similar behaviors of the skyrmion are found when $K_{uv} = 0.750$ MJ/m^3, 0.775 MJ/m^3, and 0.825 MJ/m^3. It can be found that the equilibrium position increases with increasing K_{uv}, which is shown in Fig. 3e. Periodical wavy trajectories and similar dependence of the equilibrium position on K_{uv} can be also found in the case of $j = 20$ MA/cm^2, as shown in Fig. 3d. The equilibrium positions of the periodical wavy trajectories is larger compared to the case of $j = 15$ MA/cm^2.

Fig. 4 shows the trajectories of the skyrmion in a nanotrack with sinusoidal dependence of K_u on the position x. The profile of K_u is shown in Fig. 4a. K_{u0} is the minimum and K_{uv} is the maximum. It can be found from Fig. 4b that the skyrmion moves in a sinusoidal trajectory when $K_{uv} \neq 0.8$ MJ/m^3. Differently from the case of the wedge-shaped profile of K_u, the equilibrium positions in y direction for various K_{uv} are almost the same, $y = 60$ nm. When the current density increases to $j = 20$ MA/cm^2, similar results can be found. Further, the effect of the phase also has been simulated and the results are shown in Fig. 5.

The shape of skyrmion is inversely proportional to the anisotropy which has been shown
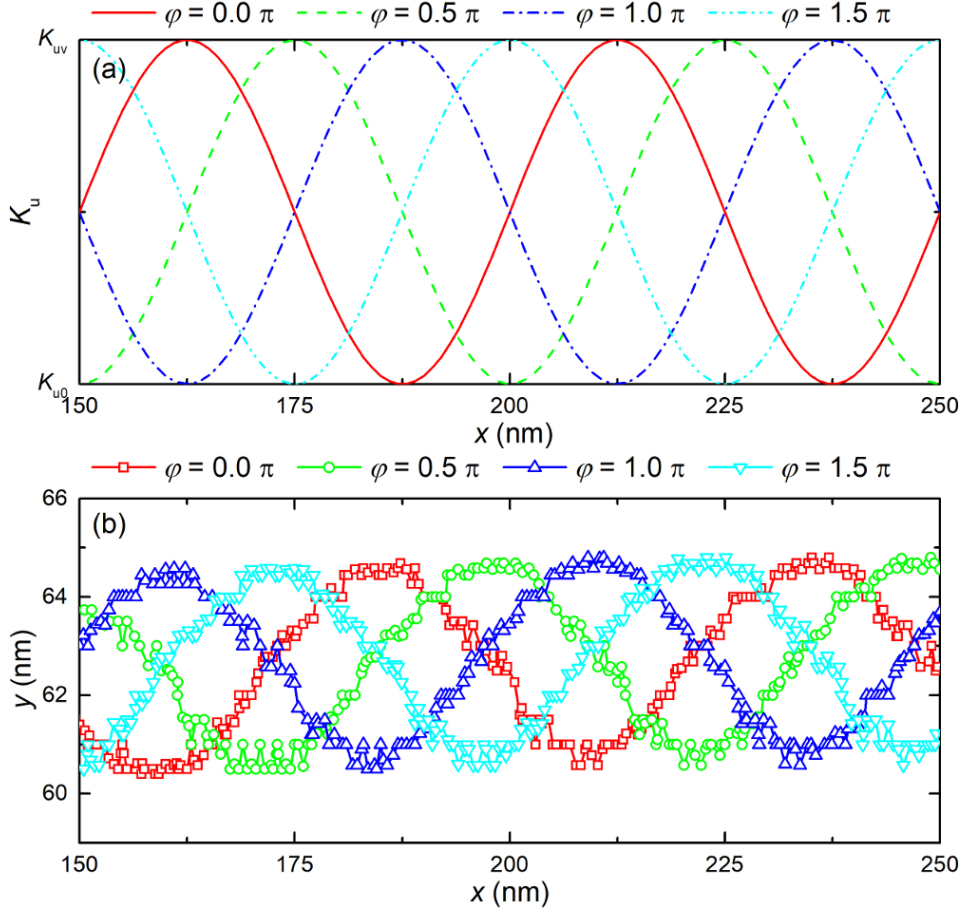
Figure 5. (a) The profile of K_u and (b) the corresponding trajectories of the skyrmion in the nanotrack with $\varphi = 0, 0.5\pi, 1.0\pi, 1.5\pi$. The driving current density is 20 MA/cm^2 applied along $+x$ axis and $K_{uv} = 0.850$ MJ/m^3.

in Fig.S1.(See Supplement Material)As shown in Fig.S1, the variation of anisotropy constant will influence the size of skyrmion. The diameter of the skyrmion is inversely proportional to the anisotropy and the diameter of the skyrmion decrease slowly after the anisotropy constant larger than 0.70 MJ/m^3. In this paper, we consider the skyrmion motion in a nanowire with K_{uv} from 0.75 MJ/m^3 to 0.85 MJ/m^3 which only has a tiny shape variation of skyrmion. The top-view of the skyrmion motion in the nanowire with a slope profile has been given in Fig.S2 which the anisotropy only induces weak impact on the shape of the skyrmion.(See Supplement Material)

In Fig. 3 - 5, the skyrmion has a transversal motion in the y direction which is influenced by the collective effect of Magnus force and edge force. The Magnus force drives the skyrmion from the center of the nanowire to the edge and depressed by the force between the momoents at the edge of the nanotrack. The Magnus force in the y component is depending on the velocity of the skyrmion in x direction[38] and the velocity of skyrmion motion in x axis V_x and y axis V_y are given in Fig. 6. When the skyrmion move to a place with a lower magnetic anisotropy, the velocity of skyrmion in x direction will increase and the Magnus Force in y component increase. The skyrmion will be driven to the edge until the Magnus
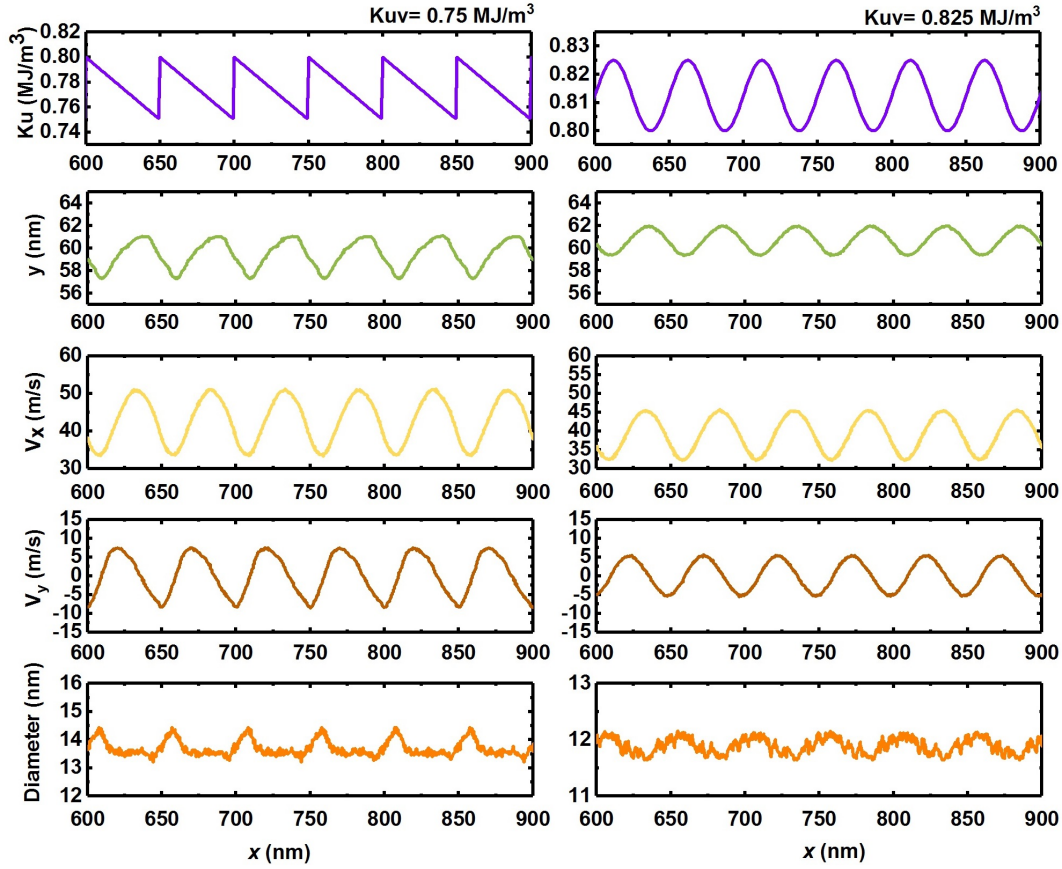
Figure 6. Movement of Skyrmion in nanotrack with slope profile and sinusoidal profile. The K_{uv} of the wedge-shaped profile is 0.75 MJ/m^3 and for the sinusoidal profile is 0.825 MJ/m^3. The driving current density is $j = 15$ MA/cm^2. The K_{uv} profile, trajectory, skyrmion velocity in x direction, skyrmion velocity in y direction and diameter of the skyrmion are given in the figure.

Force and the Edge Force is in a balance. When the skyrmion moves in a nanowire with increasing magnetic anisotropy, the velocity of skyrmion decreases and the skyrmion reduces to the center of the nanowire. This Phenomenon shows the nanowire with VCMA gate can avoid the skyrmion destroy at the edge. On the other hand, when the skyrmion moves in a nanotrack with increasing PMA, the skyrmions velocity decreases. Correspondingly, the Magnus force decreases, the skyrmion is pushed toward the center of the nantrack. Then, both repulsion and magnus force decrease, leading to that the skyrmion size increases.

3.3. Skyrmion motion driven by current pulse in nanotrack with VCMA gate

The motion of the magnetic skyrmion in the nanotrack with VCMA driven by the current pulse also be simulated. The initial position the skyrmion is $x = 86$ nm which is the middle of a voltage gate. Fig. 7 shows the motion of the skyrmion in the nanotrack with a periodical wedge-shaped profile with $K_{uv} = 0.750$ MJ/m^3 with the period length $w = 50$ nm. The current density of the pulse is 20 MA/cm^2. The pulse is applied at $t = 0.5$ ns. For one period
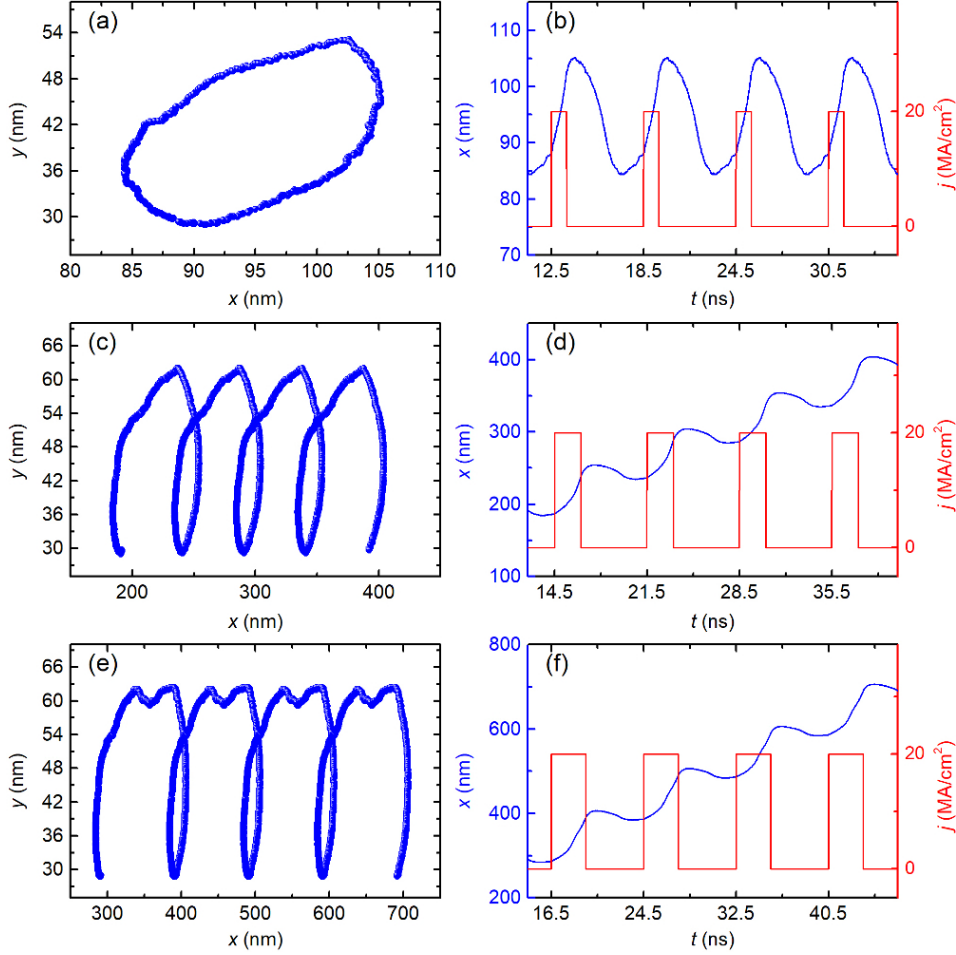
Figure 7. The skyrmion motion driven by the current pulse in the nanotrack with the wedge-shaped K_u with $K_{uv} = 0.75$ MJ/m^3. The left panel shows the trajectories of the skyrmion. The right panel shows the x position of the skyrmion and the current density as functions of time t. For one period of the current pulse , t_e is the pulse time and t_r is the relax time without applying current. $t_r = 5$ ns in the simulations. (a), (b) $t_e = 1$ ns. (c), (d) $t_e = 2$ ns. (c), (d) $t_e = 3$ ns.

of the current pulse , t_e is the time interval applying the current and t_r is the relax time without applying current. $t_r = 5$ ns in the simulations. When $t_e = 1$ ns, the skyrmion cannot pass the voltage gate and moves in a circle trajectory as shown in Figs. 7a and b. For $t_e = 2$ ns, the trajectory of the skyrmion is shown in Fig. 7c. The time-dependence of the position in the x direction and the current density are shown in Fig. 7d. At $t = 14.5$ ns, the skyrmion is located at $x = 187$ nm. After applying the pulse, $x = 241$ nm at $t = 16.5$ ns. Then the applied current is off. The skyrmion further relax to $x = 236$ nm before the next pulse. The displacement of skyrmion is 50 nm after a pulse is applied. For $t_e = 3$ ns, Figs. 7e and f, one current pulse results in a displacement of 100 nm.

Fig. 8 shows the results for the case of wedge-shaped K_{uv} with $K_{uv} = 0.850$ MJ/m^3 and the period length $w = 50$ nm. The current density of the pulse is 20 MA/cm^2 and the pulse is applied at $t = 0.5$ ns with $t_r = 5$ ns. In the Figs. 8a and b, compared with the state with K_{uv}
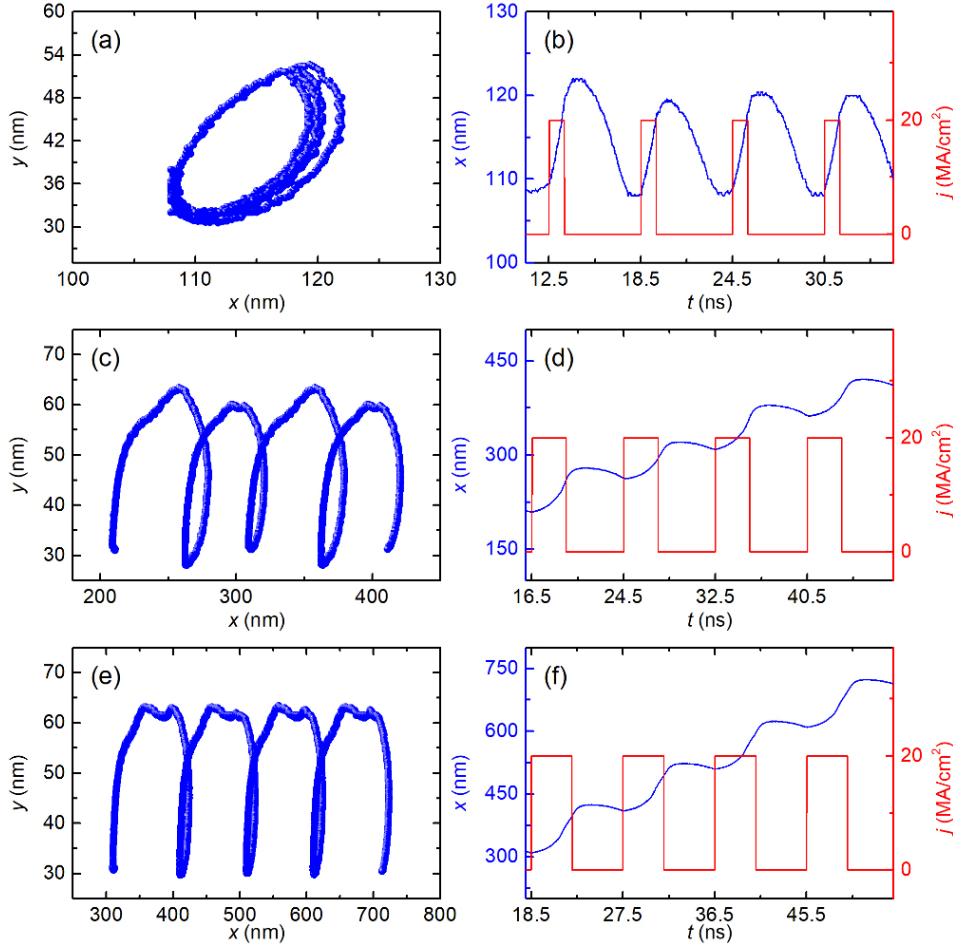
Figure 8. The skyrmion motion driven by the current pulse for the wedge-shaped K_u with $K_{uv} = 0.85$ MJ/m^3. The left panel shows the trajectories of the skyrmion. The right panel shows the x position of the skyrmion and the current as functions of time t. $t_r = 5$ ns in the simulations. (a), (b) $t_e = 1$ ns. (c), (d) $t_e = 3$ ns. (c), (d) $t_e = 4$ ns.

= 0.750 MJ/m^3, the skyrmion can more easily pass the voltage gate. This state also has been explained in the Fig. 2c. The skyrmion passes the first voltage gate and cannot pass the second voltage gate. Then the skyrmion moves in a circle trajectory. When the $t_e = 2$ ns and 3 ns, the states is similar as the Figs. 7c-f. The skyrmion passes one or two voltage gates are shown in the Figs. 8c-f. In Figs. 8c and d, for $t_e = 2$ ns, the skyrmion is located at $x = 212$ nm when $t = 16.5$ ns. After applying the pulse, skyrmion moves to $x = 277$ nm. When the current is off, the skyrmion further relaxes to $x = 263$ nm before the next pulse. The displacement of skyrmion is 50 nm after a pulse is applied. For $t_e = 3$ ns, as shown in Figs. 8e and f, one current pulse lead to a displacement of 100 nm.

Fig. 9 shows the motion of the skyrmion in the nanotrack with a sinusoidal function profile with $K_{uv} = 0.850$ MJ/m^3 with the period length $w = 50$ nm. The trajectories of skyrmion with $t_e = 1$ ns are shown in the Fig. 9a and b. The skyrmion cannot pass the voltage gate and moves in a circle which is like the Figs. 9a and b. For $t_e = 2$ ns, the trajectory of the skyrmion is shown in Fig. 9c. The time-dependence of the position in x direction and the
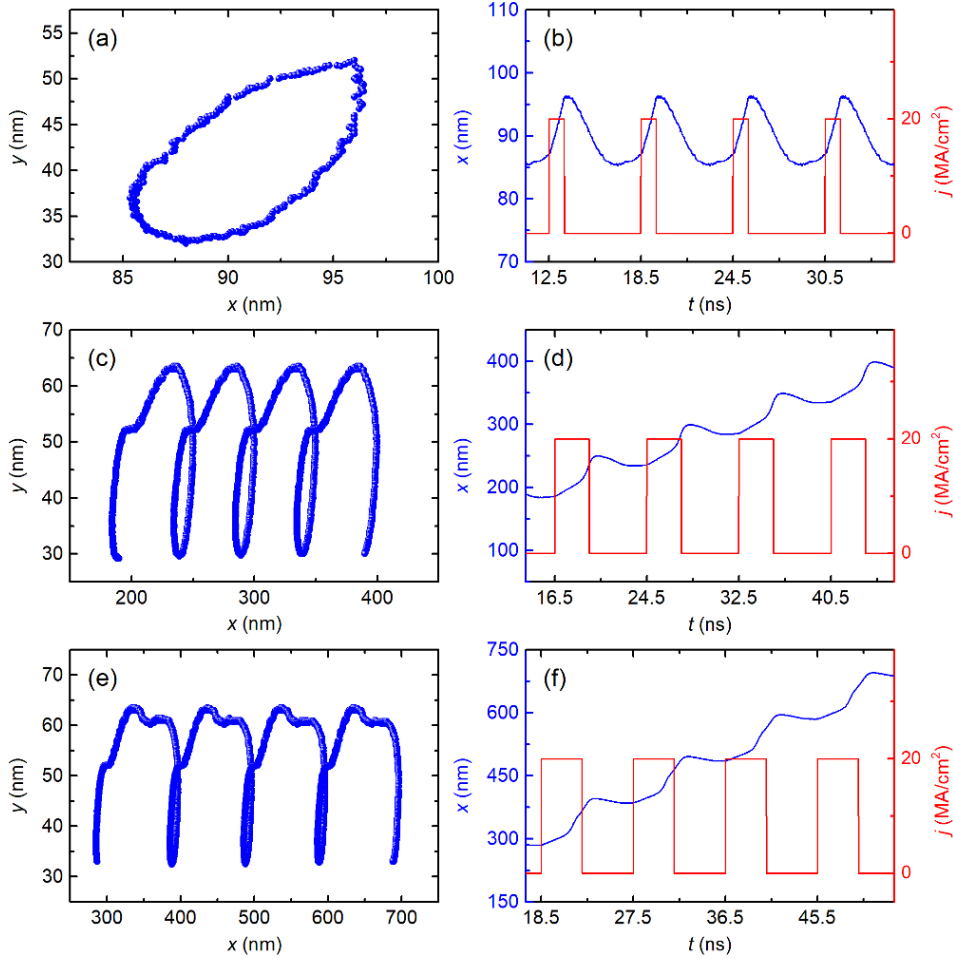
Figure 9. The skyrmion motion driven by the current pulse for the sinusoidal K_u with $K_{uv} = 0.85$ MJ/m^3 and $\varphi = 0$. The left panel shows the trajectories of the skyrmion. The right panel shows the x position of the skyrmion and the current as functions of time. $t_r = 5$ nm in the simulations. (a), (b) $t_e = 1$ ns. (c), (d) $t_e = 3$ ns. (c), (d) $t_e = 4$ ns.

current density are shown in Fig. 9d. At $t = 16.5$ ns, the skyrmion is located at $x = 186$ nm. After applying the pulse, $x = 236$ nm at $t = 18.5$ ns. Then the applied current is off. The skyrmion further relax to $x = 234$ nm before the next pulse. The skyrmion moves with a pulse time $t_e = 3$ ns is shown in Figs. 9e and f which one current pulse results in a displacement of 100 nm. From Fig. 7 to Fig. 9, it can be seen that the model with multiple voltage gates can be used to realize high density racetrack memory device.

4. Conclusions

In this paper, the skyrmion motion in a ferromagnetic nanotrack with single or multiple VC-MA gates is studied. This work shows the trajectory and location of the skyrmion can be controlled by periodically located VCMA gates as well as the driving current pulse. The u-nidirectional motion of the skyrmion realized by the VCMA effect can be used to build the skyrmion-based one-way information channel and the skyrmion diode. Our results are useful

for the design and development of the skyrmion-based spintronic devices.

See supplementary material for the deformation of skyrmion due to the variation of PMA.

Acknowledgments

References

[1] S. Mühlbauer, B. Binz, F. Jonietz, C. Pfleiderer, A. Rosch, A. Neubauer, R. Georgii, and P. Böni, Science **323**, 5916 (2009).

[2] C. Pfleiderer, T. Adams, A. Bauer, W. Biberacher, B. Binz, F. Birkelbach, P. Böni, C. Franz, R. Georgii, M. Janoschek, F. Jonietz1, T. Keller, R. Ritz, S. Mühlbauer, W. Münzer, A. Neubauer, B. Pedersen, and A. Rosch, J. Phys.: Condens. Matter **22**,16 (2010).

[3] W. Münzer, A. Neubauer, T. Adams, S. Mühlbauer, C. Franz, F. Jonietz, R. Georgii, P. Böni, B. Pedersen, M.Schmidt, A. Rosch, and C. Pfleiderer, Phys. Rev. B **81**, 041203 (2010).

[4] X. Z. Yu, N. Kanazawa, Y. Onose, K. Kimoto, W. Z. Zhang, S. Ishiwata, Y. Matsui, and Y. Tokura, Nat. Mater. **10**, 106-109 (2011).

[5] S. Heinze, K. Von Bergmann, M. Menzel, J. Brede, A. Kubetzka, R. Wiesendanger, G. Bihlmayer, and S. Blügel, Nat. Phys. **7**, 713 (2011).

[6] S. Seki, X. Yu, S. Ishiwata, and Y. Tokura, Science **336**, 198 (2012).

[7] G. Chen, A. Mascaraque, A. T. N'Diaye, and A. K. Schmid, Appl. Phys. Lett. **106**, 242404 (2015).

[8] S. Do Yi, S. Onoda, N. Nagaosa, and J. H. Han, Phys. Rev. B **80**,054416 (2009).

[9] N. Nagaosa and Y. Tokura, Nat. Nanotech. **8**, 899 (2013).

[10] A. Fert, V. Cros, and J. Sampaio, Nat. Nanotech. **8**, 152 (2013).

[11] X. Yu, Y. Tokunaga, Y. Kaneko, W. Zhang, K. Kimoto, Y. Matsui, Y. Taguchi, and Y. Tokura, Nat. Commun. **5**, 3198 (2014).

[12] H. Du, J. P. DeGrave, F. Xue, D. Liang, W. Ning, J. Yang, M. Tian, Y. Zhang, and S. Jin, Nano Lett. **14**, 2026 (2014).

[13] H. Du, R. Che, L. Kong, X. Zhao, C. Jin, C.Wang, J. Yang, W. Ning, R. Li, C. Jin, X. Chen, J. Zang, Y. Zhang, M. Tian, Nat. Commun. **6**, 8504 (2015).

[14] W. Jiang, P. Upadhyaya, W. Zhang, G. Yu, M. B. Jungfleisch, F. Y. Fradin, J. E. Pearson, Y. Tserkovnyak, K. L. Wang, O. Heinonen, S. G. E. te Velthuis, A. Hoffmann, Science **349**, 283 (2015).

[15] W. Kang , Y. Huang , C. Zheng, W. Lv, N. Lei, Y. Zhang, X. Zhang, Y. Zhou, W. Zhao, Sci. Rep. **6**, 23164 (2016)

[16] W. Kang, C. Zheng, Y. Huang, X. Zhang, Y. Zhou, W. Lv, and W. Zhao, IEEE Electron Device Letters **37**, 924 (2016)

[17] W. Kang, Y. Huang, X. Zhang, Y. Zhou, and W. Zhao, Proceedings of the IEEE **104**, 2040 (2016).

[18] W. Kang, Y. Ran, Y. Zhang, W. Lv, W. Zhao, IEEE. T. Nanotech **16**, 387 (2017).

[19] S. Li, W. Kang, Y. Huang, X. Zhang, Y. Zhou, W. Zhao, Nanotech **28.31**, 31LT01 (2017).

[20] Y. Nii, T. Nakajima, A. Kikkawa, Y. Yamasaki, K. Ohishi, J. Suzuki, Y. Taguchi, T. Arima, Y. Tokura, and Y. Iwasa, Nat. Commun. **6**, 8539 (2015).

[21] X. Zhang, Y. Zhou, M. Ezawa, G. Zhao, and W. Zhao, Sci. Rep. **5**, 11369 (2015).

[22] J. Wang, X. Zhang, X. Lu, J. Zhang, Y. Yan, ,H. Ling,J. Wu,Y. Zhou, and Y. Xu, Appl. Phys. Lett. **111**, 072401 (2017).

[23] X. Zhang, M. Ezawa, and Y. Zhou, Sci. Rep. **5**, 9400 (2015).

[24] X. Zhang, G. Zhao, H. Fangohr, J. P. Liu, W. Xia, J. Xia, and F. Morvan, Sci. Rep. **5**, 7643 (2015).

[25] Y. Liu, N. Lei, W. Zhao, W. Liu, A. Ruotolo, H.-B. Braun, and Y. Zhou, Appl. Phys. Lett. **111**, 022406 (2017).

[26] Y. Nakatani, M. Hayashi, S. Kanai, S. Fukami, and H. Ohno, Appl. Phys. Lett. **108**, 152403 (2016).

[27] Tomasello, R and Martinez, E and Zivieri, R and Torres, L and Carpentieri, M and Finocchio, G, Sci. Rep. **4**, 6784 (2014).

[28] J. Zang, M. Mostovoy, J. H. Han, and N. Nagaosa, Phys. Rev. Lett. **107**, 13 (2011).

[29] W. Jiang, X. Zhang, G. Yu, W. Zhang, X. Wang, M. B. Jungfleisch, J. E. Pearson, X. Cheng, O. Heinonen, K. L. Wang, Y. Zhou, A. Hoffmann, and S. G. E. te Velthuis, Nat. Phys. **13**, 162 (2017).

[30] Y. Keisuke, M. Soh and N. Yoshinobu, Appl. Phys. Lett. **108**, 202405 (2016).

[31] K. Haruka, Y. Kihiro, A. Fuyuki, K. Masashi, K. Tomohiro , K. Sanghoon, M. Takahiro, C. Daichi and O. Teruo, Jpn. J. Appl. Phys. **56**, 050305 (2017).

[32] X. Wang, W. L. Gan, J. C. Martinez, F. N. Tan, M. B. A. Jalilc and W. S. Lew, Nanoscale. **10**, 733 (2018).

[33] J. Franken, H. Swagten, and B. Koopmans, Nat. Nanotech. **7**, 499(2012).

[34] L. Sánchez-Tejerina, Ó. Alejos, and E. Martínez, V. Raposo, arXiv preprint arXiv:1705.00905 (2017).

[35] M. J. Donahue and D. G. Porter, *OOMMF User Guide, Version 1.0*, Interagency Report NIST IR 6376, Gaithersburg, MD (1999).

[36] S. Woo, K. M. Song, H.-S. Han, M.-S. Jung, M.-Y. Im, K.-S. Lee, K. S. Song, P. Fischer, J.-I. Hong, J. W. Choi, B. -C. Min, H. C. Koo, J. Chang, arXiv preprint arXiv:1705.09019 (2017).

[37] R. Wiesendanger, Nat. Rev. Mater. **1**, 16044 (2016).

[38] Y. Zhang, S. Luo, B. Yan, J. Ou-Yang, X. Yang, S. Chen, B. Zhu and L. You, Nanoscle. **9**, 10212 (2017).